CIENCIA 6(1), 58-76, 1998
Maracaibo, Venezuela

# Effect of the electronic structure on the electrical resistivity of Indium-Lead and Indium-Thallium diluted alloys

*Ney José Luiggi A.* and Marisol Gómez R.*
*Laboratorio de Física de Metales, Departamento de Física, Escuela de Ciencias*
*Universidad de Oriente, Apdo. Postal 299. Cumaná, Estado Sucre, Venezuela*

Recibido: 13-10-97 Aceptado: 30-03-98

## Abstract

The incidence of different approaches to the Fermi surface of pure indium, indium-thallium and indium-lead diluted alloys on the residual electrical resistivity has been evaluated in the pseudopotential model. Fermi surface, iterative transport relaxation time and correlated parameters are evaluated in the 8-OPW scheme and all transport integrals are numerically executed using the method of finite elements. The modified Heine-Animalu-Abarenkov scattering potential was used. The particular effects of the scattering of the conduction electrons on the second-zone hole and the third-zone electron β-arm for each Fermi surface (FS) considered were tested, the contribution of the scattering in the second-zone being dominant over other contributions. Our results are in agreement with the experimental ones when the relativistic FS approach is used.

**Key words:** Electrical resistivity; electronic structure; Indium diluted alloys.

# Efecto de la estructura electrónica sobre la resistividad eléctrica de aleaciones diluidas de Indio-Plomo e Indio-Talio

## Resumen

Hemos evaluado la resistividad eléctrica residual de aleaciones diluidas indio-talio e indio-plomo en el modelo de pseudopotencial, tratando de dilucidar el efecto que tiene sobre esta propiedad la consideración de diferentes aproximaciones de cálculo de superficies de Fermi. Estos parámetros correlacionados y el tiempo de relajación determinado iterativamente, son evaluados en el esquema, 8-OPW, calculándose todas las integrales de transporte mediante el método de elementos finitos. El potencial dispersor usado es el de Heine-Animalu-Abarenkov el cual es parametrizado a fin de considerar detalles propios del proceso de aleación. El efecto particular de la dispersión de los electrones de conducción en la segunda zona de huecos y en la rama-β de la tercera zona de electrones para cada SF considerada fue chequeado, siendo dominante la contribución de la dispersión en la segunda

* To whom correspondence should be addressed. E-mail: nluiggi@sucre.udo.edu.ve. Phone: 58-93-513592. Fax: 58-93-513592.

zona. Nuestros resultados están en concordancia con los resultados experimentales reportados en la literatura cuando usamos una SF calculada en la aproximación relativista.

**Palabras clave:** Aleaciones diluidas de Indio; estructura electrónica; resistividad eléctrica.

## Introduction

The study of transport coefficients of metals and alloys has been the subject of much research, fundamentally, because those coefficients permit us to obtain information in regards to specific characteristics of the studied materials. In the specific case of residual coefficients, particular attention has been paid to the scattering of the conduction electrons as a result of impurities. Despite the elastic behavior of electron-impurity interaction, the calculation of these coefficients presents formidable difficulties that can only be overcome by using different models and approaches.

First, we must select a model to describe the scattering of conduction electrons by impurities between the pseudopotential model (PM) (1) and the Korringa-Koster-Green function (KKR) (2) method. Choosing the former introduces the limitations of the Born approach, such as the non-consideration of the contribution of the backscatterers to the total scattering, though the calculation is facilitated as it allows the independent appraisal of both the effect of the structural distribution and the scattering power of impurities. The free parameters of the PM approach guarantee an agreement between the measured and the calculated transport coefficients.

Choosing the latter allows for less physical restrictions but the incorporation of certain effects such as those of lattice distortion (3,4) demands grater effort on the part of the researchers. The KKR uses the muffin-tin potential to describe the host metal and impurity cluster scattering potentials entering into the KKR formalism through a partial-wave phase shift (5).

Second, we must select an FS. Again, the problem is reduced to the competition between PM-OPW (6) and the cellular methods (7,8), where the differences are basically introduced by the crystalline waves function used. Both comprise an ample spectrum of atomic hosts, the first one being of little use when transition atomic hosts are considered. In the pseudopotential model in particular, and depending on the calculation assumptions used (9-11), the FS of the host metal under study indium - presents topological differences that must certainly influence the residual transport coefficients.

In this work we use the pseudopotential method with the phenomenological potential of Heine-Animalu-Abarenkov for the scattering. With the purpose of knowing the effect of the electronic structure on the residual resistivity of pure indium, In-Tl and In-Pb diluted alloys, the Fermi surface and correlated parameters are evaluated through both a relativistic and a non-relativistic approach in the case of the former, and from a relativistic approach in the last two.

The organization of this paper is as follows: Chapter 2 introduces the aspects pertaining to residual resistivity and FS. Chapter 3 sets forth the method of calculations and finally chapter 4 presents the results and discussion.

## Theoretical aspects

### Indium diluted alloys

The diluted alloys studied in the present work have an indium matrix as host metal. The indium crystallizes in the tetragonal system, its Bravais lattice being face centered. Like aluminium, indium is lo-

cated in the III A group of the periodic table, having one p and two s electrons of valence, electronic configuration which allows us to use the same methods as those employed with aluminium,

Having two s and two p electrons of valence, lead is a substitutive impurity in indium; and thallium being isoelectronic with indium, is also substitutional. The changes of indium. lattice parameters due to the inclusion of the impurities have been studied by Holthman et al. (10) who have reported mathematical expressions of these parameters as functions of the atomic concentration of impurities, where the electronic and size effects are considered. In the case of thallium, only the size effect is important. Table I schedules the parameters of the In-Pb and In-Tl alloys used in this work.

**Residual electrical resistivity**

The electrical conductivity tensor σ is defined in the theoretical framework given by the transport Boltzmann equation as one integral over the FS of the alloy, the integrand one function being dependant on both the electronic velocity vector $\upsilon(k)$ and the electronic mean free path vector $\lambda(k)$. Because of the tetragonal symmetry of indium, the components of the conductivity tensor in *plane z = constant* are equal, *i.e* $\sigma_{xx} = \sigma_{yy}$, and different from the tensor component $\sigma_{zz}$ perpendicular to that plane. The inversion of the σ tensor permits us to define the anisotropic electrical resistivity ρ (3).

$$\varrho_i^{-1} = \sigma_{ii} = \frac{e^2}{4\pi^3\hbar}\int_{FS} \upsilon_i(k)\lambda_i(k)\frac{ds_k}{\upsilon(k)} \qquad [1]$$

where the subscript *i* takes the values *x* or *z* to define the parallel or perpendicular electrical resistivity to plane *z*. The transport equation also provided an equation to relate vectors $\upsilon(k)$ and $\lambda(k)$,

$$\upsilon(k)\cdot E = \int_{FS} P(k,k')(\lambda(k)-\lambda(k'))\cdot E dk' \qquad [2]$$

where $P(k, k')$ is the transition probability between the electronic states k and k', the vector mean free path being independent of the direction of the applied electric field E. The analytical solution of integral equation [2] is not simple in practice, and for that reason an iterative solution is proposed [11]

$$\lambda(k) = \tau_0(k)[\upsilon(k) + \int_{FS} \lambda(k'))P(k,k')dk'] \qquad [3]$$

where $\tau_0$, the average lifetime of electrons, is the inverse of the electron-impurity rate scattering,

$$\tau_0 = [\int_{FS} P(k,k')dk']^{-1} \qquad [4]$$

Another relation between v(k) and λ (k), which expedites the solution of equation [1] is obtained introducing an anisotropic relaxation time $\tau_p$, appropriate to resistivity,

$$\tau_p(k) = \frac{\upsilon(k)\cdot\lambda(k)}{\upsilon(k)\cdot\upsilon(k)} \qquad [5]$$

where the particular condition of parallelism between these vectors is valid only for an isotropic system with a spherical FS. Fundamentally the definition of $P(k, k')$ permits us to establish the differences indicated in the introduction regarding the scattering of conduction electrons by impurities. $P(k, k')$ is related to the impurities concentration C, the number of sites in the alloy N and the transition matrix $T(k, k')$ by,

$$P(k,k') = 2\pi NCT(k,k')^2\delta(E_{k'} - E_k) \qquad [6]$$

where

$$T(k,k') = \langle\psi(k)|V(r)|\psi(k')\rangle$$

In the Born approximation, the T matrix approaches the $V(k, k')$ matrix, where the electronic wave function is a plane wave or a combination of plane waves. Surely, this approach is valid for metals and alloys where the electronic conduction is guaranteed for s and p electrons, but is not true when localized electrons participate in the conduction processes.

A detailed study on the evaluation of $P(k, k')$ in the KKR model is presented in the works by Coleridge (13,14) and Mertig et al. (15). In our case the electronic wave function is written in the n-OPW model

$$|\psi_k\rangle = \sum_i^n a_k \, |k - g_i\rangle \qquad [7]$$

where $g_i$ is a reciprocal lattice vector and n fixes the wave number necessary to split the degeneration introduced by symmetry effects.

When $P(k, k')$ is known, an approach of zero order of $\lambda(k)$ in equation [3] is necessary to evaluate equation [1]. An excellent one is obtained using the Ziman approximation, which in the n-OPW model is written:

$$\lambda^0(k) = v(k)\frac{\Omega_0 C}{4\pi^2\hbar}\int_{FS}\left|\sum_n\sum_{n'} a_n(k)a_{n'}(k')\,\Delta V(Q_{n,n'})\right|^2 (1-\cos\Theta_{k,k'})\frac{ds'}{|\nabla_{k'}E|} \qquad [8]$$

where $Q_{n,n'} = k' - k + g_n + g_{n'}$ and

$$\Delta V(Q_{n,n'}) = \langle k' - g_{n'}|\Delta V(r)|k - g_n\rangle$$

is the form factor. This factor defines the scattering power or interaction potential between the impurity atoms and the host.

## Impurity scattering pseudopotentials

The scattering potential is evaluated from the following relation (16,17)

$$\Delta V(Q) = \frac{\varepsilon_i\Omega_i}{\varepsilon_h\Omega_h} V_i\left(Q\frac{k_F^i}{k_F^h}\right) - V_h(Q)[1 - \Delta S(Q)] \qquad [9]$$

where subscripts $i$ and $h$ refer to the impurity and host atoms. $\varepsilon$ represents the dielectric constant of Hartree and $\Omega$ the respective atomic volumes. $\Delta S$ is the structural change introduced by the impurity atoms in the indium. host matrix. V identifies the pseudopotential of both the host of pure indium and the host of impurities respectively. The prefactor in the first right term of equation [9] serves to normalize the impurity matrix to the host matrix. In this work we use the modified Heine-Animalu-Abarenkov pseudopotential for $V_i$ and $V_h$. Animalu and Heine (6), following a quasi-phenomenological pseudopotential model calculated the form factors of a group of elements which have been tabulated in reference (6). Our personal experience has demonstrated (18) that the direct use of that pseudopotential in the calculation of residual resistivity in aluminium. alloys generates results in disagreement with the experience; however, the very minor changes introduced in equation [9] permit us to parametrize that relation,

$$\Delta V(Q) = \frac{\varepsilon_i\Omega_i b_1}{\varepsilon_h\Omega_h} V_i\left(b_2\frac{Qk_F^i}{k_F^h}\right) - b_3 V_h(Q)\,[1 - \Delta S(Q)] \qquad [10]$$

where $b_i$ ($i$ = 1, 2,3) are parameters close to one, and have been phenomenologically calculated. The deformation contribution in equation [9] is evaluated according to Fukai (16) and Harrisson (6), by means of the expression:

$$\Delta S(Q) = A\left[\frac{1}{\Omega_h}\frac{d\Omega}{dc}\right]Q \qquad [11]$$

where

$$A = -\frac{5}{12\pi}\frac{C_{11}+2C_{12}}{3C_{11}+2C_{12}+4C_{44}}\gamma\Omega_s \left[\sum_i^M n_i\frac{J_1(Q|r_i|)}{ri^2} + 4\pi\frac{J_0(Q|r_M|)}{\Omega_s Q}\right] \qquad [12]$$

where $C_{ij}$ constitutes the elastic stiffness constant of the host matrix, $\gamma = 3\frac{(1-\sigma)}{(1-\sigma)}$, $\sigma$ being the Poisson coefficient of the indium host; $\frac{d\Omega}{dc}$ the change of atomic volume per unit of impurity; $r_i$ the radius of the i-th atomic shell and $n_i$ the number of atoms in that shell.

Another pseudopotential frequently used to calculate transport properties is the Aschroft local pseudopotential (9); however, a preliminary study (19) using it generated results of a smaller magnitude than those observed in the experience.

## Electronic structure and Fermi surface

The transport integrals are evaluated on the FS and for that reason it is necessary to know the real FS. Particularly for indium. we find two discrepant topologies of its FS in the literature. The first, designed non-relativistic Fermi surface, introduced by Aschroft et al., (9) presents a closed second-zone hole and a third-zone electron arranged in a β-arm in the ⟨110⟩ direction and an α-arm in the ⟨101⟩ direction. The second, named relativistic Fermi surface (20,21), considers the spin-orbit interaction and discards the α-arm, the third zone of the FS appearing as a ring around the X symmetry point.

In this section we briefly present the pseudopotential formulation for the evaluation of the electronic structure and the FS of indium and indium diluted alloys.

The hamiltonian $H$ of our system is written as

$$H = \frac{p^2}{2m} + V(r) + V_{s-o}\delta_{s,o} \qquad [13]$$

where $V(r)$ represents the crystalline potential and $V_{s-o}$ is the potential associated to the spin-orbit interaction. $\delta_{s,o}$ is a delta function which leads us to the relativistic approach if $\delta_{s,o} = 1$ and to non-relativistic approach if $\delta_{s,o} = 0$.

$$V_{s-o} = \left(\frac{1}{2}\alpha_f^2\right) \nabla V(r) \times p \cdot \sigma \qquad [14]$$

where $\alpha_f$ is the structure fine constant, $p$ is the linear momentum operator and σ is the Pauli Spin operator.

The hamiltonian equation is solved in the OPW methods by assuming a crystalline wave function which is a combination of OPW,

$$H|\psi_k(r,s)\rangle = E(k)|\psi_k(r,s)\rangle \qquad [15]$$

where

$$|\psi_k(r,s)\rangle = \sum C_g(k)[I - P_c O]|k-g,s\rangle \qquad [16]$$

where $P_c$ is an operator projecting the core wave function upon the wave vector space when the spin is not considered. The 0 operator introduces the spin effect in equation [16],

$$O = I(I^s - I)\delta_{s,o} \qquad [17]$$

$I$ and $I^S$ being the identity operator in the wave vector space and the spin space respectively. Using equations [13] and [14] we obtain the secular equation which permits us to evaluate the band electronic structure and the FS in the non-relativistic and relativistic approaches.

$$\begin{aligned}\langle k',s'|H - E|k,s\rangle &= (k^2 - E_k)\delta_{k,k'}\delta_{s,s'} + \\ &U_g S_g \delta_{k-k'}\delta_{s,s'} + \\ &\langle k',s'|V_{s-o}|k,s\rangle\,\delta_{s,o}\end{aligned} \qquad [18]$$

where $U_g$ is the Fourier transform of the crystalline potential, and $S_g$ the structure factor of the crystalline unitary cell.

The matrix elements associated with the spin-orbit interaction have been widely evaluated in the literature (20-22),

$$\begin{aligned}\langle k',s'|V_{s-o}|k,s\rangle = &-iC_{n',nl}D_{n',l'k'}D_{n,l}(k)S_g\delta_{k-k',g} \\ &(\hat{k}' \times \hat{k})\langle s'|\sigma|s\rangle\end{aligned} \qquad [19]$$

where

$$C_{n',nl} = \int_0^r R_{n'l}(r)\xi(r)R_{n,l}(r)r^2 dr \qquad [20]$$

$$D_{n,l}(k) = \int_0^r J_l(kr)R_{n,l}(r)r^2 dr \qquad [21]$$

$$\xi(r) = \frac{1}{2}\alpha_f^2 \frac{1}{r}\frac{\delta V}{\delta r} \qquad [22]$$

$R_{n,l}$ is the radial wave function to the atomic core, and $J_l$ is the l-order spherical Bessel function. The right-side of equation [17] must include a sum for each subscript $n$ and $l$; however, the overlap integrals $D_{n,l}$ are dominant for the (n,l) pairs, namely (4,1), (5,1) and (5,1), corresponding to indium, thallium and lead respectively.

## Computational aspects

### Electronic structure and Fermi surface

The electronic structure and the FS are calculated by equation [16], in the first case, fixing the wave vector $k$ and increasing the electronic energy $E$ to obtain the $E$ values that avoid the secular equation, and in the second, fixing the energy on to the Fermi level and varying the wave vector $k$ up to accomplish the same previous condition. For the non-relativistic calculation the energy was varied with steps of 0.08 mryd while the wave vector step was of 0.0002 au, $E$ or $\vec{k}$ generating a secular determinant smaller than or equal to $10^{-10}$ au being considered as solution for the secular equation. For the relativistic aproximation, the use of the hamiltonian operator resulted computationally cumbersome presenting complex terms, the algorithms being different from those used in the previous case, although the precision of the calculation was maintained.

**1. Non-relativistic approach:** This approach is determined completely by $\delta_{s,o} = 0$ in equation [16] and considering the $U_{\vec{g}}$ parameters as known quantities. Luiggi (11) studied the effect of the $U_{\vec{g}}$ parameters on the FS, choosing the two parameter sets proposed by Aschroft et al. (9) to study indium and using 8-OPW as the wave function. The parameters used in this work are scheduled in Table 1. The direct effect of lead and thallium impurities is not considered in this approach.

**2. Relativistic approach:** This approach corresponds to equation [16] with $\delta_{s,o} = 1$. The fact of considering the spin contribution duplicates the number of terms in the wave function, the secular equation being twice as large as the one obtained in the non-relativistic approach. The parameters for indium and diluted alloys are selected from those proposed by Holthman (20) and Holthman et al. (10). Those parameters are shown in Table 1. All calculation details appear in reference (11).

Our calculations in indium permit us to confirm that the FS and the electronic structure are sensitive to:

Table 1
Parameters of indium and indium diluted alloys, used in the relativistic and non-relativistic electronic structure and Fermi surface calculations

| | Non-Relativistic | Relativistic | | |
|---|---|---|---|---|
| | In | In | In 0.522% at Pb | In 1.060% at Tl |
| $E_f$ (ua) | 0.63838 | 0.64178 | 0.64203 | 0.64160 |
| $k_f$ (ua) | 0.79899 | 0.80111 | 0.80127 | 0.80100 |
| U(1,1,1) | 0.04419 | -0.05510 | 0.05531 | 0.05515 |
| U(0,0,2) | -0.01845 | -0.02299 | -0.02343 | -0.02297 |
| U(2,0,0) | 0.00241 | 0.01797 | 0.01780 | 0.01772 |
| U(2,0,2) | 0.05603 | | | |
| U(1,1,3) | 0.06198 | | | |
| U(2,2,0) | 0.05878 | | | |
| U(3,1,1) | 0.06158 | | | |

Table 2
Electronic energy calculated on high symmetry points of the first Brillouin zone, showing changes introduced by impurities when the relativistic approach is used

| Simmetry point | Indium | In 0.522% at Pb | In 1.060% at Tl |
|---|---|---|---|
| Γ | -0.00804 | -0.00804 | -0.00804 |
| | 1.48392 | 1.47912 | 1.46952 |
| X | 0.47752 | 0.47672 | 0.47752 |
| | 1.03028 | 1.04227 | 1.04068 |
| | 1.05184 | 1.04784 | 1.04784 |
| | 1.07660 | 1.08540 | 1.08406 |
| U | 0.44156 | 0.438340 | 0.43916 |
| | 0.54392 | 0.54312 | 0.54392 |
| | 0.62868 | 0.63108 | 0.63028 |
| | 1.12944 | 1.12944 | 1.12784 |
| | 1.14700 | 1.14780 | 1.14700 |
| T | 0.49276 | 0.48636 | 0.48716 |
| | 0.60952 | 0.60872 | 0.61032 |
| | 0.64868 | 0.66548 | 0.66468 |
| | 0.73904 | 0.72624 | 0.72624 |
| W | 0.54956 | 0.53916 | 0.53916 |
| | 0.61912 | 0.62392 | 0.62392 |
| | 0.63588 | 0.64868 | 0.64868 |
| | 0.77184 | 0.76384 | 0.76304 |
| N | 0.51356 | 0.51356 | 0.51356 |
| | 0.52472 | 0.51356 | 0.512312 |
| | 0.96788 | 0.98388 | 0.98468 |
| | 1.0262 | 1.0094 | 1.01024 |

- The OPW number in the wave function
- The $U_g$ values or the crystalline potential
- Whether the spin-orbit interaction is considered or not.

Also, the presence of impurities introduces changes in the host matrix, consequently changing the FS and the electronic structure; examples of these changes are presented in Table 2, where we show the electronic energy calculated in the relativistic approach at points of high symmetry in the first Brillouin zone.

Figure 1-a shows the (001) section of the FS of indium for $k_z$ = 0.00, using the non-relativistic and the relativistic approaches. It is interesting to notice the strong difference in area topology shown by each calculation approach. Figure 1b presents contour curves for a third-zone electron arm of the FS calculated in the relativistic approach. The effect of impurities on the second-zone hole in the relativistic approach is small, but it is remarkable in the third-zone electron; these effects are shown in Figure 1-b for In-Pb alloy, which are com-

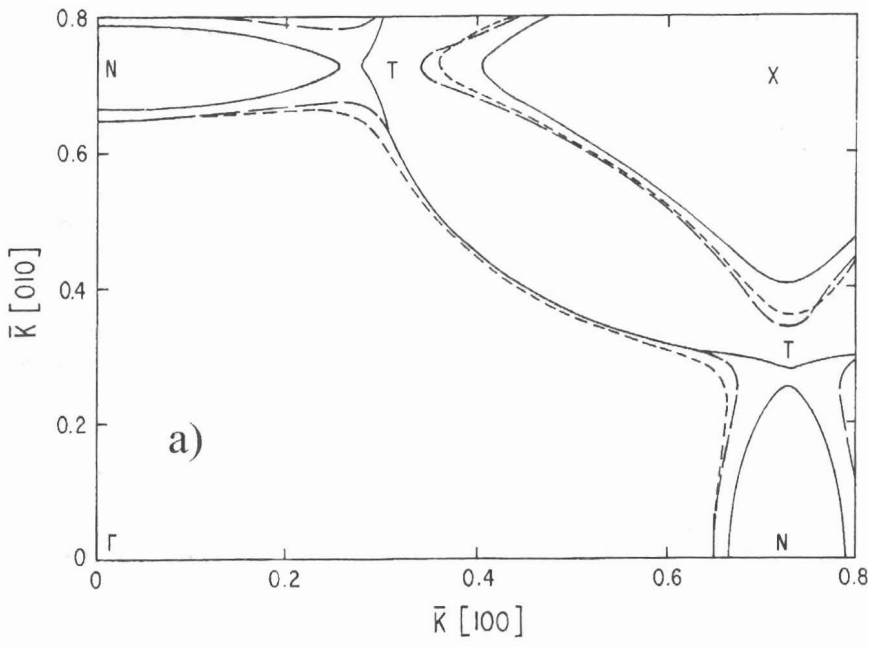


Figure 1-a. (001) section of second-hole zone of the Fermi surface of pure indium using different approaches: — — Non-relativistic approach (Set of parameters in Table 1). —— Non-relativistic approach (Second set of parameters of references (9,11)). - - - Relativistic approach (Set of parameters in Table 1).

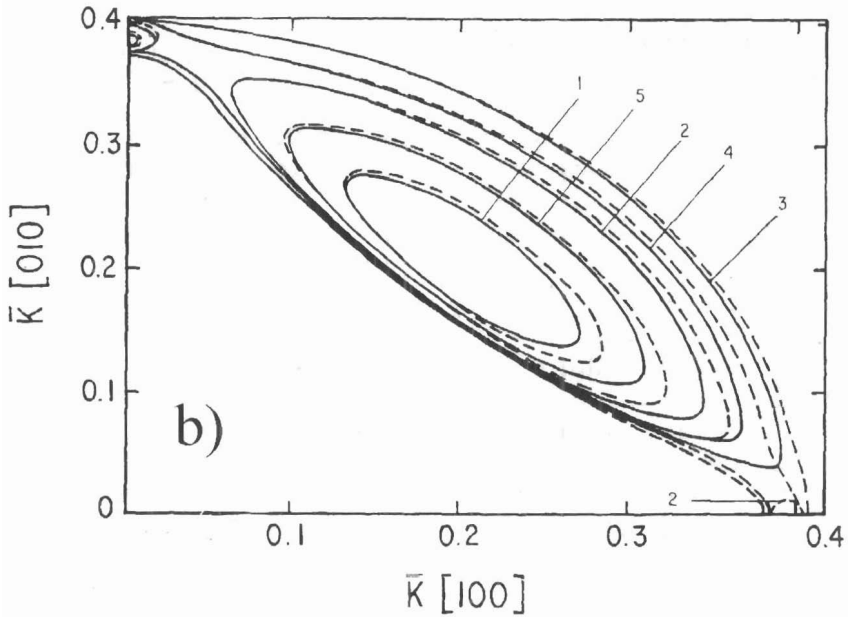


Figure 1-b. Comparison of third zone contour curves of the Fermi surface of pure indium and indium alloys. 1. $k_z = 0.62$ au 2. $k_z = 0.64$ au 3. $k_z = 0.66$ au 4. $k_z = 0.70$ au 5. $k_z = 0.72$ au. - - - Orbits of pure indium. —— Orbits of In-0.522% at. Pb.

pared with indium. We remark that, as referenced by other authors (20,21), the pure indium β-*arm* Fermi surface defines a ring around the X symmetry point; however when we include the impurities for the 8 OPW model considered in this work, slight changes are observed, the ring not always being closed.

**Correlated parameters**

The correlated parameters with the FS are mainly the electronic velocity and the wave function coefficients and must be evaluated in each point of the selected grid for each FS used.

**Wave function coefficients**: We transform our hamiltonian formulation given by equations [13-22] and [7] as a homogeneous equation system whose solution, other than the trivial one, is obtained redefining the unknowns, $a_{\vec{k}}$, as the ratio between a fixed coefficient and all others, our system of equations thus remaining as one of an order immediately inferior to the original system and soluble by the traditional methods. The normalization condition $\sum a_i^* a_i = 1$ allows us to identify each coefficient. For the non relativistic Fermi surface this method permits a complete evaluation of the eight wave function coefficients for each $\vec{k}$ considered, while for the Fermi surface calculated through the relativistic approach there will be two associated coefficients for each $\vec{g}$ vector, one for each spin value. In this case our method permits us only to determine the absolute value of the coefficients associated with each $\vec{g}$ vector. Due to the similarity between the absolute value of the non-relativistic and relativistic coefficients, the sign of the relativistic ones is taken as equal to the sign of non-relativistic coefficients.

Figure 2 shows the contour curves of some wave function coefficients projected on a (001) section of the plane containing a 1/8 of the maximum orbits of the second-zone hole FS, also shown in the figure. The $a_i$ coefficients (i = 1 and 2) for pure indium (Figure 2-a and b) and indium-thallium alloys (Figure 2-c and d) calculated on the FS in the relativistic approach are shown. We can notice in this approach the presence of contour lines not present in the previous surface. The effect of the FS and its anisotropy over the wave function can also be inferred from these figures.

Figure 3 shows the behavior of some wave function coefficients projected over the maximum orbit of the third zone in the plane containing the X point of the first Brillouin zone. Figures 3-a through 3-c correspond to the $a_i$ coefficients (i = 5, 7 and 8) using the FS of pure indium calculated in the relativistic approach, while Figures 3-d through 3-f correspond to the same coefficients using the FS of indium-lead alloy. Again, in these figures the effect of the FS on the wave functions is obvious.

**Electronic velocity:** Assuming energy as a $k_F$ function, $\vec{v}(\vec{k})$ is derived from the expression,

$$\vec{v}(\vec{k}) = \frac{1}{\hbar} \Delta_{\vec{k}} E = \frac{1}{\hbar} \sum_i^n a_i^* a_i (\vec{k} - \vec{g}_i) \qquad [23]$$

where the square modules of $a_i$ coefficients were previously evaluated, and the differences obtained for each FS considered are directly transmitted to the velocity vector. Figure 4 shows a (001) section of the projection of the velocity module for the Fermi surface portion plotted in Figure 2, corresponding to the non-relativistic approach for the FS of pure indium, the velocity band remaining defined by contour lines partitioned by the (110) plane with minimum values of velocity for $\vec{k}$ vectors close to a symmetry line or point in the first Brillouin zone. The behavior of the velocity for other approaches of the FS is similar to the one obtained through the non-relativistic approximation. In Figure 5 the velocity module projected on the third zone, as in Figure 3, is presented. In Figure 5-a, 5-b, 5-c and 5-d we use the FS of pure indium in the non-relativistic and relativistic ap-

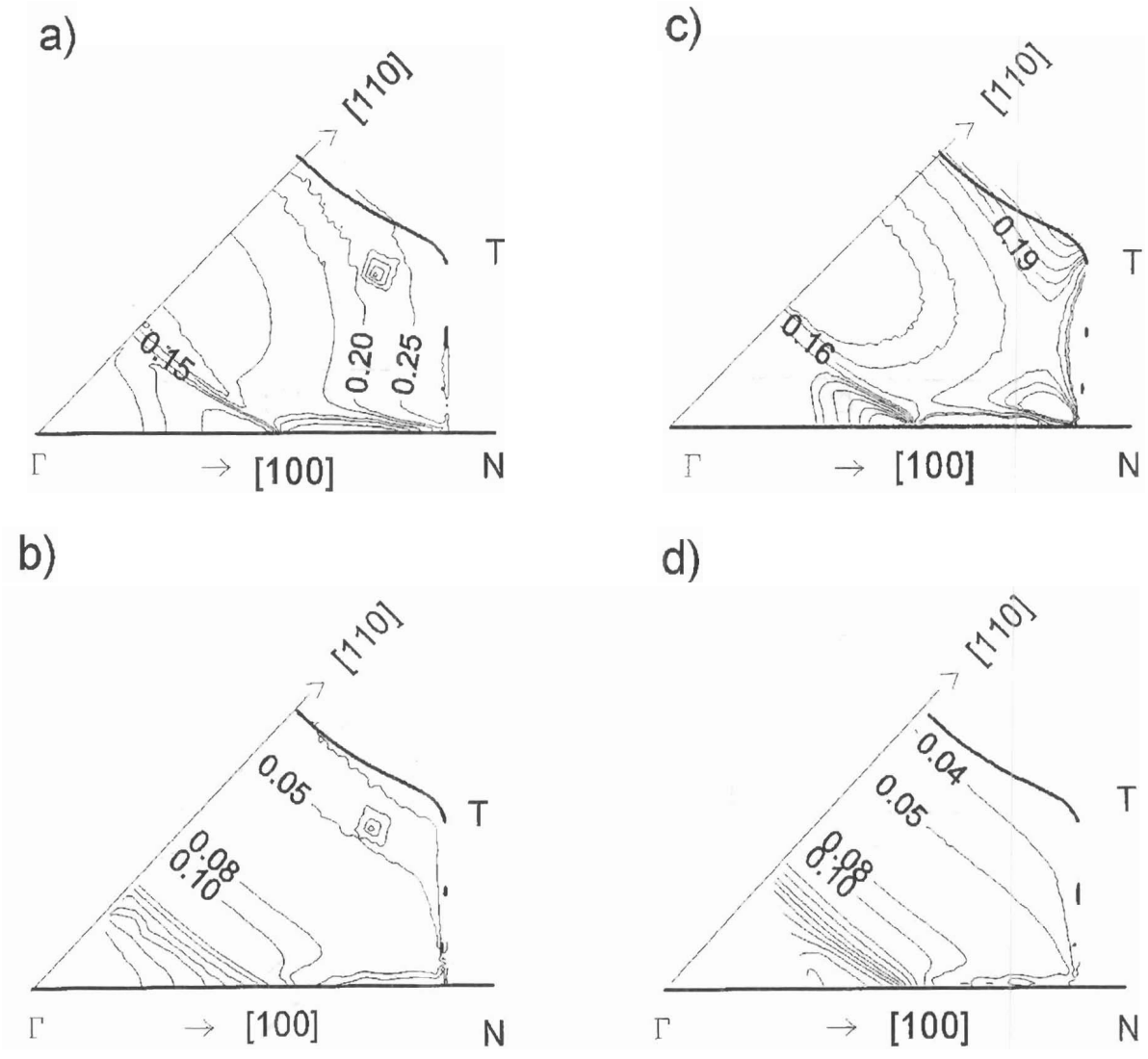


Figure 2. Wave function coefficients projected on a (001) section of the maximum orbit of the second zone (shown in gross line) for: a) $a_1$: Fermi surface of pure indium in the relativistic approach. b) $a_2$: Fermi surface of pure indium in the relativistic approach. c) $a_1$: Fermi surface of an indium-thallium alloy in the relativistic approach. d) $a_2$: Fermi surface of an indium-thallium alloy in the relativistic approach.

proaches, and the FS of In-Pb and In-Tl alloys respectively. Again, the effect of the electronic structure on this parameter is obvious.

**Integral evaluation:** $\lambda(\vec{k}')$ and $\rho(\vec{k})$ are integrals defined on the Fermi surface. These surfaces are numerically attainable with high precision and it is necessary to find a numerical method where we can optimally combine the precision and the time of calculation, which is achieved by means of the finite element method (22). The holes and electrons Fermi surfaces are covered with geometrically defined elements whose nodes are end points of $\vec{k}$ vectors and where

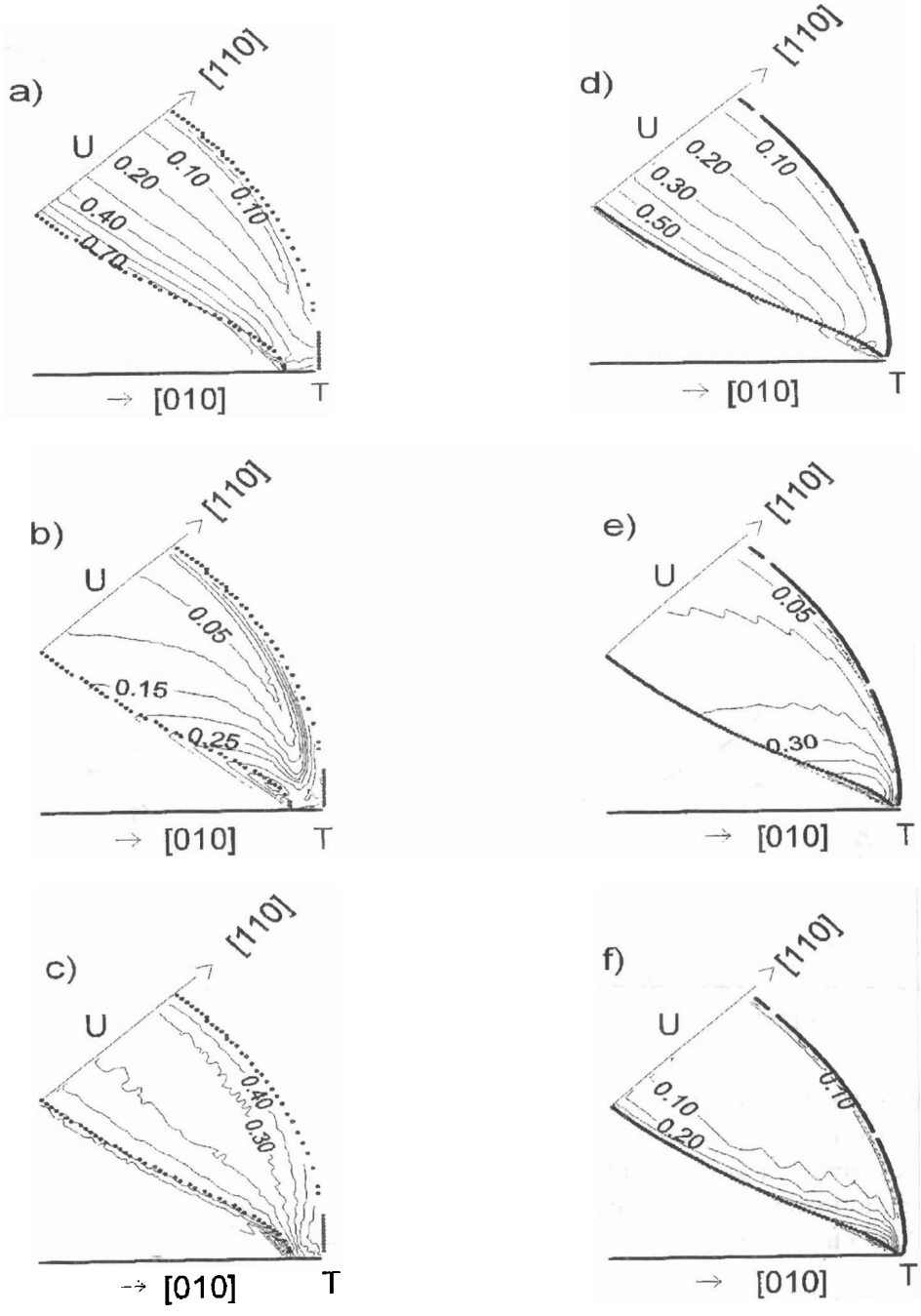


Figure 3. Wave function coefficients projected on the maximum section of a third electron zone arm (shown in gross line) for: a) $a_5$: Fermi surface of pure indium in the relativistic approach. b) $a_7$: Fermi surface of pure indium in the relativistic approach. c) $a_8$: Fermi surface of pure indium in the relativistic approach. d) $a_5$: Fermi surface of an indium-lead alloy in the relativistic approach. e) $a_7$: Fermi surface of an indium-lead alloy in the relativistic approach. f) $a_8$: Fermi surface of an indium-lead alloy in the relativistic approach.

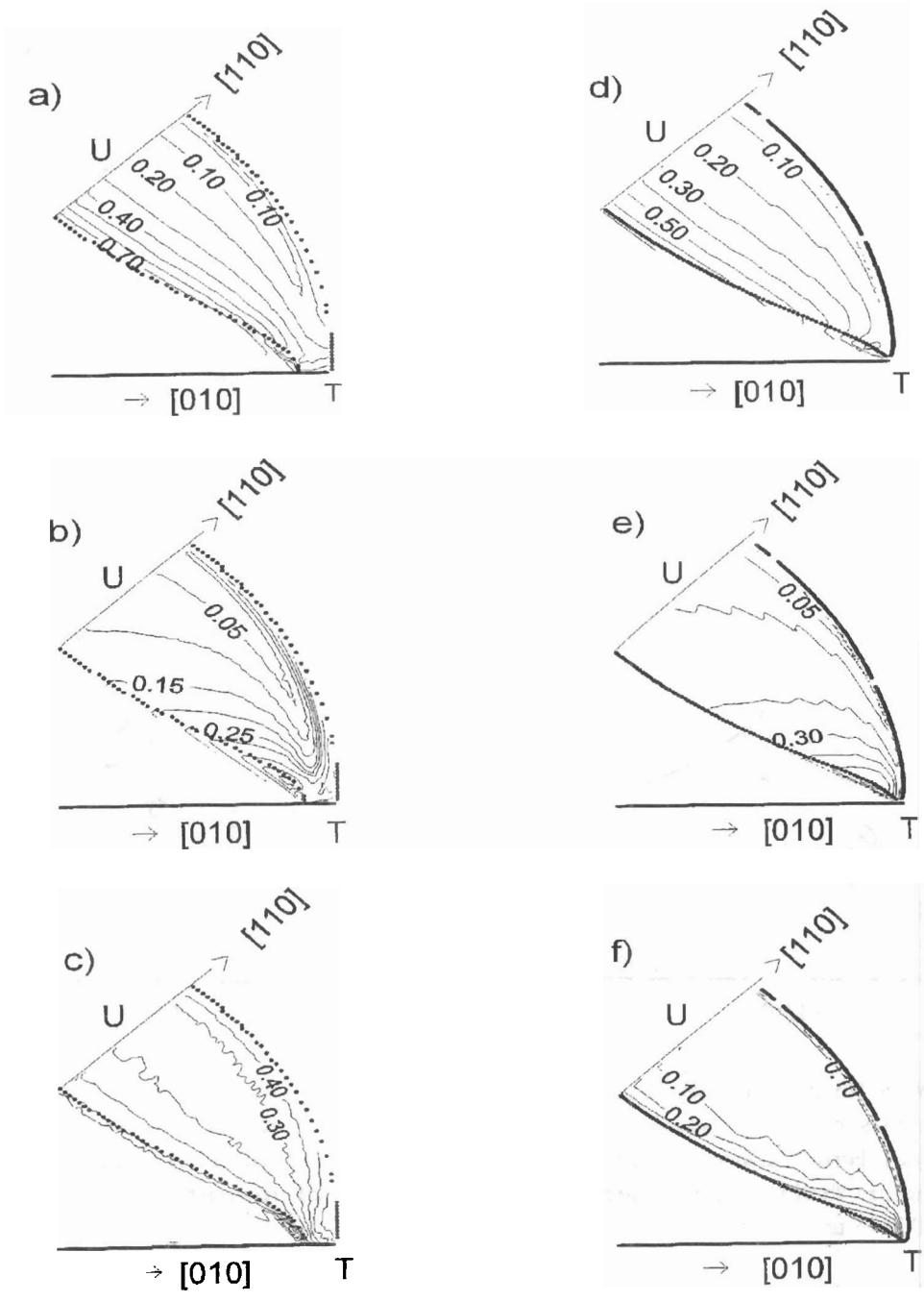


Figure 3. Wave function coefficients projected on the maximum section of a third electron zone arm (shown in gross line) for: a) $a_5$: Fermi surface of pure indium in the relativistic approach. b) $a_7$: Fermi surface of pure indium in the relativistic approach. c) $a_8$: Fermi surface of pure indium in the relativistic approach. d) $a_5$: Fermi surface of an indium-lead alloy in the relativistic approach. e) $a_7$: Fermi surface of an indium-lead alloy in the relativistic approach. f) $a_8$: Fermi surface of an indium-lead alloy in the relativistic approach.

all correlated parameters are known. We select triangular elements of three nodes and project each element upon a single reference triangle. The one to one condition to make the transformation possible is checked by means of the non-singularity of the Jacobian matrix. The utilization of 3-node triangular elements render the Jacobian independent of the transformation coordinates, so that the integration process is reduced to an analytical calculation on the diferential surface element of a triangle, added to all triangles of the integration grid. One triangularization algorithm was performed permitting us to control the number, size and direction of the node path in each triangle. The effect of the number of points and triangles in the integration grid was checked by means of the relaxation time integral, using 12.000, 6.000 and 3.000 nodes covered by 20.000, 10.000 and 5.000 triangles, thus obtaining a reduction in calculation time of 2% and 6% respectively relative to the first case, but the gain in machine time is nearly 60%. In this work we use grids of 3.000 nodes and estimate a global error of 10%.

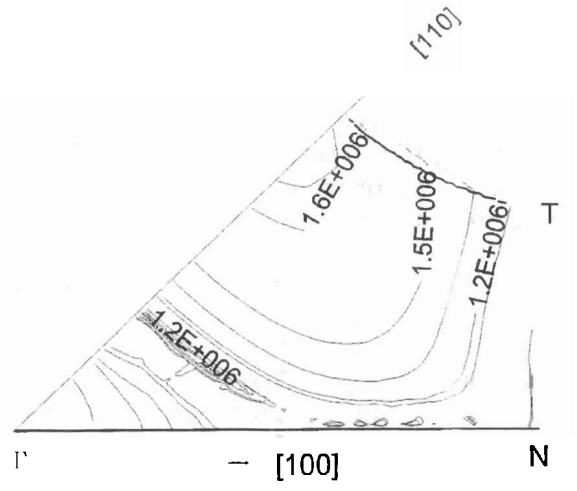


Figure 4. Velocity module projected on a (001) section of the maximum orbit of the second zone (shown in gross line) Fermi surface of pure indium in the non-relativistic approach.

## Results and discussion

### Relaxation time and electronic mean free path

The electronic mean free path, λ, given by equation [3] and its first iteration given by

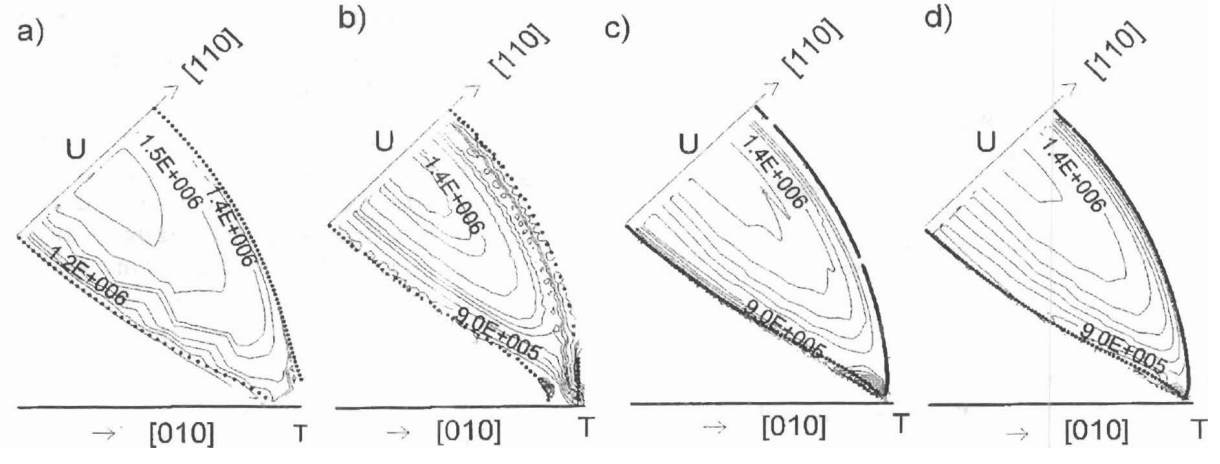


Figure 5. Velocity module projected on the maximum orbit of an arm of the third electron zone (shown in gross line) for: a) Fermi surface of pure indium in the non-relativistic approach. b) Fermi surface of pure indium in the relativistic approach. c) Fermi surface of an indium-lead alloy in the relativistic approach. d) Fermi surface of an indium-thallium alloy in the relativistic approach.

equation [81 are integrated over all the scattered $\vec{k}'$ vectors falling upon the Fermi surface. The relaxation time, $\tau$, is obtained from equation [5]. Each parameter is evaluated for thallium and lead using the FS of the studied alloy as well as the FS of pure indium calculated in the non-relativistic and in the relativistic approaches. Figure 6 depicts the relaxation time of indium-lead alloy projected on the second (Figure 6-a) and third (Figure 6-b) zones of the FS of pure indium in the nonrelativistic approach. The results reported by others authors (3) are confirmed in these figures.

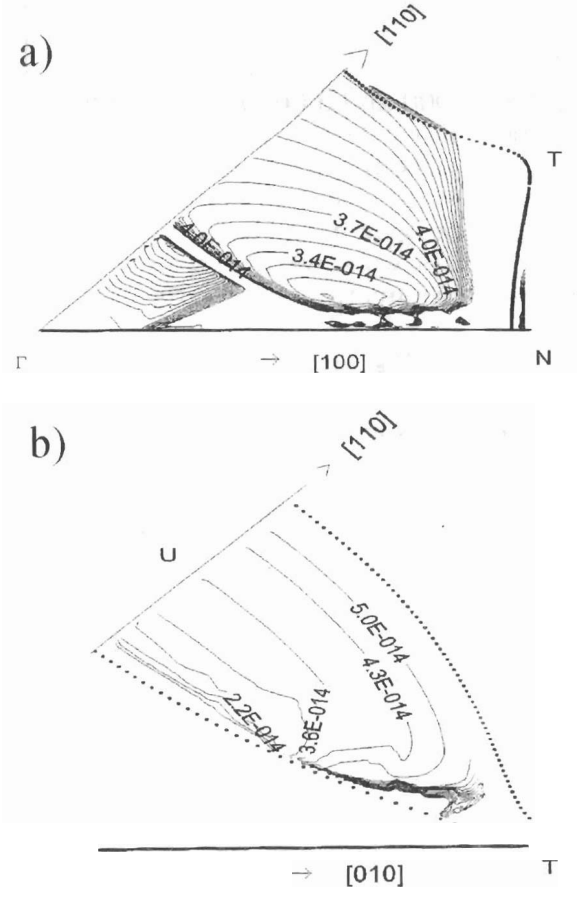


Figure 6. Relaxation time projected on a (001) section of the maximum orbit of: a) Second-hole zone (shown in gross line) of pure indium in the non-relativistic approach. b) Third-electron zone (shown in gross line) of pure indium in the non-relativistic approach.

To ease the comparison of results the converging iteration for $\lambda^x$ and $\tau^x$, for the outermost orbits in the second and third zones of the Fermi surface are plotted and identified with the subscripts "0" and "$\phi$" respectively, the orbits of the Fermi surfaces being shown in both cases. Figure 7 represents our results for the In-Pb alloy, corresponding to the relativistic Fermi surface of pure indium. Relaxation time and electronic mean free path also have been calculated using non-relativistic FS of pure indium and relativistic Fermi surface of In-Pb alloy, showing results qualitatively differents of these shown in Figure 7. We can infer from these curves the nearly free character of the electrons in great part of the second zone as evidenced by the almost constant values of $\tau$ and $\lambda$. This constant nature is lost at the high symmetry points of the first Brillouin zone, where the Fermi surface presents a curvature change. The parallelism between $\vec{v}_{\vec{k}}$ and $\vec{\lambda}_{\vec{k}}$ is also impaired at those points, by nearly a maximum of 25°, deviation which reaches 50° in the third zone.

The relaxation time anisotropy was estimated to be of a factor of 2.5, 3.2 and 3.2 for each of the Fermi surfaces considered, which can be attributed essentially to the s-type character of the electrons connecting $\vec{k}$-states and generating a strong dispersive power in the third zone, while the electrons connecting $\vec{k}$-states in the second zone are mainly of type p and have less dispersive power. We can particularly point out that, in indium, the non-relativistic FS reinforces the nearly free character of the electrons, behavior less evident in the FS of either pure indium or alloy -specially in the third zone- obtained by means of the relativistic approach. A higher resolution of the parame-

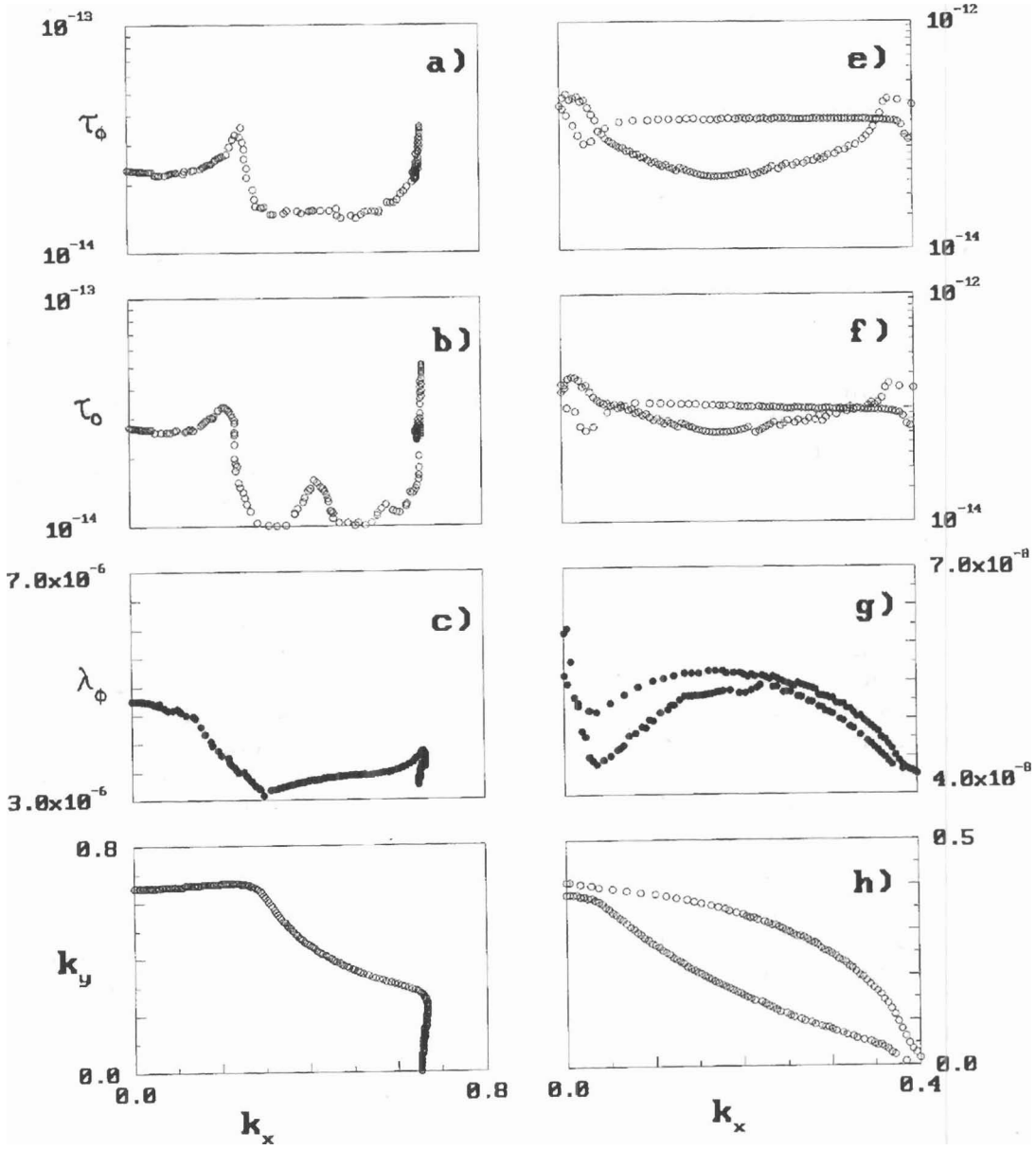


Figure 7. Relaxation time and free path mean of an indium-lead alloy calculated on the maximum orbit of the Fermi surface of pure indium in the relativistic approach. a) Relaxation time for the iteration $\phi = 3$ in the second-hole zone shown in 7-d). b) Relaxation time for the Ziman approach ($\phi$=0) in the second-hole zone shown in 7-d). c) Free path mean for the iteration $\phi = 3$ in the second-hole zone shown in 7-d). d) Maximum orbit of Fermi surface's second-hole zone. e) Relaxation time for the iteration $\phi = 3$ in the third-electron zone shown in 7-h). f) Relaxation time for the Ziman approach ($\phi$=0) in the third-electron zone shown in 7-h). g) Free path mean for the iteration 3 in the third-electron zone shown in 7-h). h) Maximum orbit of the Fermi surface's third-electron zone.

ters obtained by the non-relativistic methods is also evident, as the routine requires only a maximum of three iterations to rearch the condition for a valid convergence. On the other hand, surfaces relativistically obtained required up to ten iterative procedures to reach the condition necessary for a valid convergence, increasing the size of their hamiltonian matrices and decreasing the resolution of the studied parameters.

The effect of the dispersive potential is not shown but when we use the Aschroft potential, the relaxation time does not present qualitatively important changes compared with the HAA scattering pseudopotential, though the relaxation time may differ up till one order of magnitude, which evidences the importance of the Fermi surface in this calculation.

Figure 8 shows our results for the In-Tl alloy, corresponding to the non-relativistic FS of pure indium. The effect of another Fermi sufaces also was calculated but not shown. The behaviors of $\tau_k$ and $\lambda_k$ are similar to those obtained for In-Pb, though with a more accentuated parallelism between $\vec{v}_{\vec{k}}$ and $\vec{\lambda}_{\vec{k}}$, which reaches a maximum of 35° in the second zone and a maximum of 60° in the third zone, despite the fact that the $\tau_{maximum} : \tau_{minimum}$ ratio, which defines the anisotropy factor, is maintained at 2.8, 4.0 and 3.5 for each Fermi surface used. Also the homovalent character and the tetraghonal crystalline structure of thallium and indium, contribute to such a large anisotropy.

The observations for the In-Pb alloy are equally valid for In-Tl alloy.

**Electrical resistivity**

The results in this section are obtained integrating equation [1] over all $\vec{k}$ vectors incident upon the Fermi surface. Tables 3 and 4 show our results for In-Pb and In-Tl alloys respectively. In these tables, in addition to the resistivities in the plane, $\rho_a$, and perpendicular to that plane, $\rho_z$, we show the average resistivities obtained in light of $\langle\rho\rangle = \frac{1}{3}(2\rho_x + \rho_z)$, and the $\rho_{free}$ resistivity associated with the average relaxation time for electrons and holes evaluated by means of the free electron model, where the electron and hole numbers by surface unity are taken directly from the triangles over the Fermi surface used to calculate the properties. For In-Pb we deduce the dominant effect of the second zone over the inverse relaxation time. The resistivities seem overestimed when the non relativistic Fermi surface is used with the Ziman approach; however, in the iterative calculation, $\rho_z$ shows a monotonous decrease which ends at $\phi = 3$, the contribution parallel to the plane reamaining almost constant. We do not have a precise explanation for that variation, but the iterative process most likely prompts the participation of factors not present in the Ziman approach. The iterated $\langle\rho\rangle$ value is in agreement with the reported value (3). A factor of 3 separates the behavior of the resistivity of free electrons from the one calculated when the full Fermi surface is considered, deviation which can be associated with three causes:

1. An overestimation of $n^h$ and $n_e$ in the direct calculation of $\rho_{free}$.
2. An underestimation of the average relaxation time in the second and third zone of the Fermi surface.
3. The separation of the real Fermi surface from the spherical surface where the calculation of $\rho_{free}$ is performed.

The relativistic Fermi surface of pure indium diminishes the anisoptropy, the results being in perfect agreement with the experience after three iterative steps. A factor smaller than 2 separates the behavior of $\langle\rho\rangle$ and $\rho_{free}$ this possibly being due to the consideration of the spin-orbit interaction in the FS evaluation.

The results obtained using the Fermi surface of In-Pb alloys are also adequate

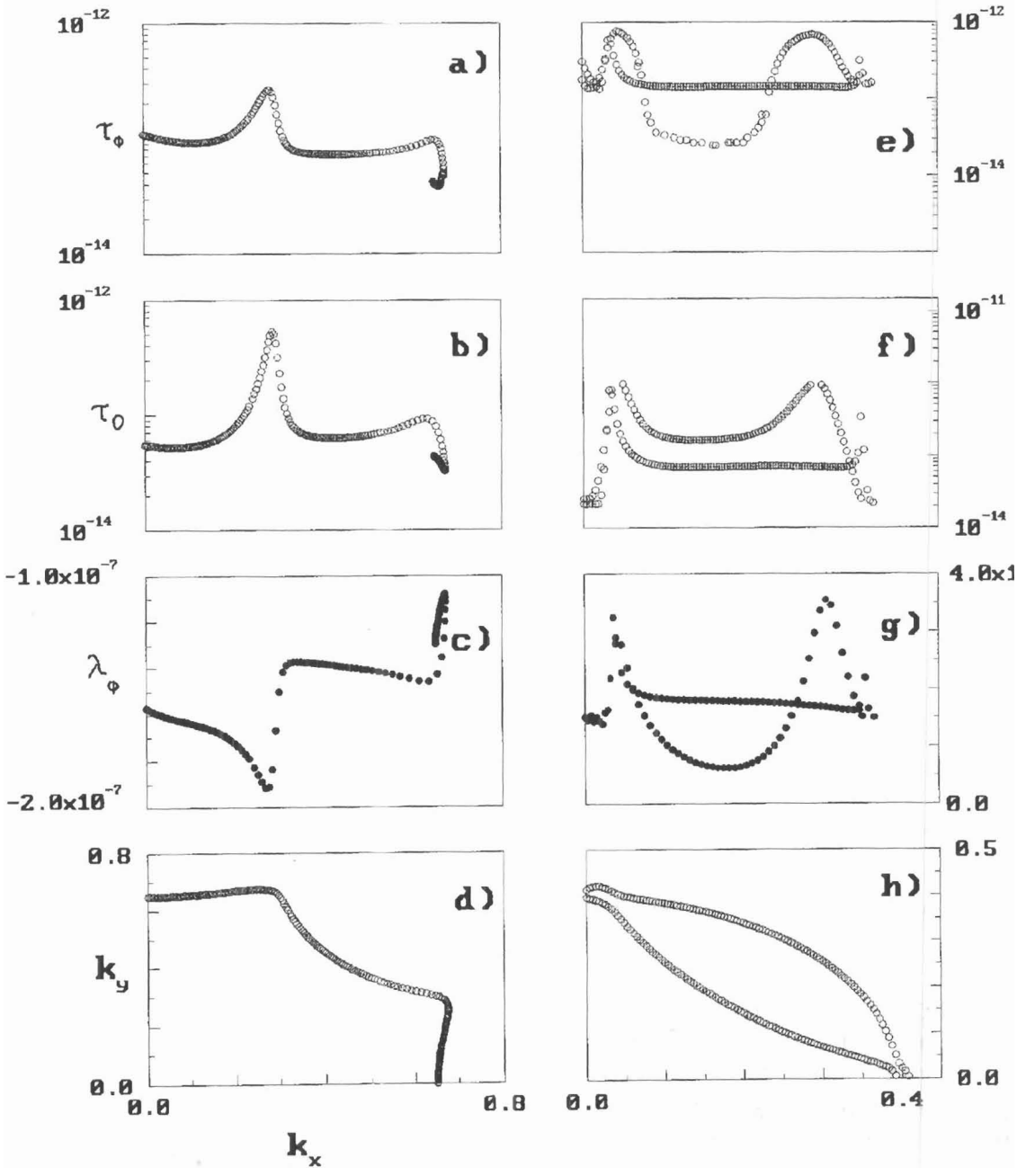


Figure 8. Relaxation time and free path mean of an indium-thallium alloy calculated on the maximum orbit of the Fermi surface of pure indium in the nonrelativistic approach. Same legend as that of Figure 7. The $\phi$ value is 3.

Table 3
Anisotropic residual resistivities (μΩ*cm/at*%) and average inverse relaxation time ($s^{-1}$) in the second and third zones of the Fermi surface for an In-Pb alloy

| FS | Nº | $\langle\tau_h\rangle^{-1}$ | $\langle\tau_e\rangle^{-1}$ | $\rho_z$ | $\rho_a$ | $\langle\rho\rangle$ | $\rho_{free}$ | published data |
|---|---|---|---|---|---|---|---|---|
| PINR | 0 | $3.50x110^{13}$ | $0.82x10^{13}$ | 1.44 | 0.65 | 1.18 | 0.31 | 0.51-0.60[a] |
| | ϕ | $1.90x\ 10^{13}$ | $0.75x10^{13}$ | 0.28 | 0.73 | 0.59 | 0.18 | |
| PIR | 0 | $3.70x\ 10^{13}$ | $1.10x10^{13}$ | 0.48 | 0.68 | 0.62 | 0.38 | 0.44[b] |
| | ϕ | $3.55x\ 10^{13}$ | $0.99x10^{13}$ | 0.42 | 0.63 | 0.56 | 0.36 | |
| Alloy | 0 | $2.96x\ 10^{13}$ | $1.07x10^{13}$ | 0.31 | 0.320 | 0.34 | 0.34 | |
| | ϕ | $4.81x\ 10^{13}$ | $0.95x10^{13}$ | 0.39 | 0.53 | 0.48 | 0.59 | |

[a]Reference (3,24). [b]Reference (23).

Table 4
Anisotropic residual resistivities (μΩ*cm/at*%) and average inverse relax-ation time ($s^{-1}$) in the second and third zones of the Fermi surface for an In-T1 alloy

| FS | Nº | $\langle\tau_h\rangle^{-1}$ | $\langle\tau_e\rangle^{-1}$ | $\rho_z$ | $\rho_a$ | $\langle\rho\rangle$ | $\rho_{free}$ | published data |
|---|---|---|---|---|---|---|---|---|
| PINR | 0 | $0.39x10^{13}$ | $0.16x10^{13}$ | 0.14 | 0.38 | 0.30 | 0.10 | 0.18-0.21[a] |
| | ϕ | $0.53x10^{13}$ | $0.13x10^{13}$ | 0.17 | 0.43 | 0.35 | 0.10 | |
| PIR | 0 | $0.33x10^{13}$ | $0.07x10^{13}$ | 0.15 | 0.23 | 0.21 | 0.14 | 0.08[b] |
| | ϕ | $0.30x10^{13}$ | $0.06x10^{13}$ | 0.14 | 0.23 | 0.20 | 0.14 | |
| Alloy | 0 | $0.24x10^{13}$ | $0.11x10^{13}$ | 0.12 | 0.13 | 0.12 | 0.09 | |
| | ϕ | $0.25x10^{13}$ | $0.18x10^{13}$ | 0.15 | 0.20 | 0.19 | 0.13 | |

[a]Reference (3). [b]Reference (23).

though slightly lower than those calculated using the Fermi surface of pure indium, the $\rho_{free}$ being very simjilar to that of $\langle\rho\rangle$. Again, the explanation of this fact must be found in a combination of the factors previously mentioned.

In Table 4, the $\langle\rho\rangle$ value for In-Tl is calculated with the non-relativistic Fermi surface yielded once more an overestimated resistivity; however, the $\rho_{free}$ value was in the theoretical range reported by Ruiter et al. (3). The results with the relativistic Fermi surface for pure indiurn and the alloy are in agreement with the experiments (23,24).

## Conclusions

The residual electrical resistivities of the In-Pb and In-Tl alloys have been calculated using the 8-OPW scheme. The effect of different approaches for the calculation of a real Fermi surface and correlated parame-

ters on these surfaces has been tested, verifying that:

1. Different Fermi surface approaches produce topological changes capable of introducing important variations of the correlated parameters which affect the properties associated with them.

   The transport coefficients are very sensitive to the scattering potential the $b_i$ parameters of equation [10] being equal to (1.0,1.0, 0.75) and (1.0, 1.0, 0.88) for In-Pb and In-Tl alloys respectively. The potentials of the core model of Aschroft (9) for both alloys were tested generating results of up till one order of magnitude lower than those obtained with the HAA potential.

3. For a same scattering potential (HAA) the Fermi surface calculated in the non relativistic approach over-estimates the residual resistivity value. This behavior can possibly be associated with the presence of α-arms in the third zone of the Fermi surface, arms which are not considered in this calculation, while the calculations in the relativistic scheme for both alloys generate results in agreement with the experience.

4. As a zero order approach, the Ziman approximation yields results which, even for this tetraghonal structure, are very close to those reported experimentally (23,24).

## Acknowledgments

This work was supported by the Consejo de Investigación de la Universidad de Oriente, under project CI-5-022-00541/93 and by CONICIT, under projects S1-950000844. We also want to acknowledge our appreciation to Carlos Mota and his company TRADUCE, C.A., for the review of this manuscript.

## References

1. SORBELLO R. ***J Phys F: Metal Phys*** 14: 1655-1683, 1974.
2. LODDER A., BARATTA G.A., RIJSDIJK' G.A. ***J Phys F: Metal Phys*** 18:1057-1068,1978.
3. RUITTER J.C.C. ***Physika B*** 154:140-151, 1989.
4. LODDER A. ***J Phys F: Metal Phys*** 6:1885-1897, 1976.
5. VAN E.K., LODDER A. ***Physics Letters A*** 144(6,7):379-384, 1990.
6. HARRISON W.A. ***Pseudopotentials in the Theory of Metals.*** W.A. Benjamin. New York (USA), pp. 1-123, 1966.
7. LOUCK T.L. ***Augmented Plane Wave Method,*** W.A. Benjamin, New York (USA), pp. 123, 1966.
8. SINGH D. ***Plane Waves, Pseudopotentials and the LAPW Method,*** Kluwer Academic Publisher, Boston (USA), pp. 17-43, 1994.
9. ASCHROFT N.W., LAWRENCE W.E. ***Phys Rev*** 175(3):938-955, 1968.
10. HOLTHMAN P.M., PRIESTLEY M.W. ***J Phys F: Metal Phys*** 1:621-637, 1971.
11. LUIGGI N.A. ***Acta Científica Venezolana*** 45:186-198, 1994.
12. Taylor P.L. ***A Quantum Approach to the Solid State,*** Prentice Halls, New Jersey (USA), pp. 15-67, 1970.
13. COLERIDGE P.T. ***J Phys F: Metal Phys*** 2: 1016-1031, 1972.
14. COLERIDGE P.T. ***J Phys F: Metal Phys*** 15: 1727-1739, 1985.
15. MERTING I., MROSAN E., ZELLER R., DEDERICHS P.H. ***Phys Status Solidi*** (b) 119:251-260,1983.
16. FUKAI Y. ***Phys Rev*** 186:697-704, 1969.
17. LUIGGI N.J., FEBRES 0. ***Phys Rev B*** 46: 1992-2000, 1992.
18. LUIGGI N.J., SIMON J.P., GUYOT P. ***J Phys F: Metal Phys*** 10:865-877, 1980.

19. GÓMEZ M., LUIGGI N.J. (unpublished).
20. HOLTHMAN P.M. ***J Phys F: Metal Phys*** 6: 1457-1479, 1976.
21. SOVEN P. ***Phys Rev*** 137-6A: A 1706-1717, 1964.
22. DHATT G., TOUZOT G. ***The Finite Element Method Displayed,*** John Wiley & Sons: New York (USA), pp. 18-42, 1984.
23. ALEKSANDROV B.N., DUKIN V.V. ***Sov J Low Temp Phys*** 2:54-63, 1976
24. BRONNIKOV A.D., VOL'SKII E.P., PETRASHOV V.S., TSOI V.S. ***Sov Phys JETP*** 40: 357-365, 1974.